High-energy-density polymeric carbon oxide: Layered C_xO_y solids under pressure

Chuli Sun,[1] Wei Guo,[1,2,3,*] Jinlong Zhu,[4,5,†] Xiang Li,[1,2] and Yugui Yao[1,2,3]

[1]*Key Laboratory of Advanced Optoelectronic Quantum Architecture and Measurement (MOE), School of Physics, Beijing Institute of Technology, Beijing 100081, People's Republic of China*

[2]*Frontiers Science Center for High Energy Material (MOE), Beijing Institute of Technology, Beijing 100081, China*

[3]*State Key Laboratory of Explosion Science and Technology, Beijing Institute of Technology, Beijing 100081, China*

[4]*Department of Physics, Southern University of Science and Technology, Shenzhen 518055, China*

[5]*Center for High Pressure Science and Technology Advanced Research (HPSTAR), P.O. Box 8009, Beijing 100088, China*

(Received 6 July 2021; accepted 24 August 2021; published 7 September 2021)

HPSTAR 1241-2021

Pressure-induced polymerization of carbon monoxide (CO) molecules may lead to next-generation high energy density materials. By combining structural search method, first-principles calculations and *ab initio* molecular dynamics (AIMD) simulations, we predict several polymeric carbon oxide C_xO_y, i.e., C_5O_2 (P-4m2), C_6O_4 (P-4m2 and I-4m2) and C_8O_8 (I-4m2), which are all layered semiconductors with high energy density, large bulk modulus, and high hardness. For the C : O ratio = 1 : 1, the C_8O_8-I-4m2 phase is energetically more stable than the reported *Cmca* and *Cmcm* phases above 90 GPa, and its energy density is 4.51 kJ/g, which is higher than trinitrotoluene (TNT). Considering the mechanism of CO_2 release, $C_xO_y(x > y)$ crystals, namely C_5O_2 (P-4m2) and C_6O_4 (P-4m2 and I-4m2) are predicted above 40 ∼ 50 GPa. At 100 GPa, phonon spectrum calculations and AIMD simulations indicate that they have good mechanical and dynamic stability. At 0 GPa, AIMD simulations also show the possible phase transition path of the four C_xO_y structures by releasing CO_2: C_8O_8-I-4m2 → C_6O_4-I-4m2 and C_6O_4-P-4m2 → C_5O_2-P-4m2, and C_6O_4-I-4m2 and C_5O_2-P-4m2 can remain stable at ambient conditions. Those structures may enrich the phase diagram of high-pressure C_xO_y, and provide clues for synthesis and exploration of new stable energetic materials besides polymeric nitrogen.

DOI: 10.1103/PhysRevB.104.094102

I. INTRODUCTION

As a new type of material, polymeric solids with low-Z elements have attracted the attention of researchers for their unique properties such as high energy density [1–4], super hardness [5,6] and superconductivity [7]. Therefore, polymeric carbon monoxide (CO) [8,9], N_2 [10,11], CO_2 [12,13], O_2 [14] and their mixtures have been intensively studied. CO and N_2 molecules are isoelectronic, they have the strongest heteronuclear or homonuclear bond (triple bond), the same total mass number and a similar phase diagram [15,16]. When their polymers, composed of single or double bonds, decompose into triple bonds, a large amount of energy is released, so they are considered as candidates of next-generation high energy density materials (HEDM). In addition, CO is abundant in interstellar medium, it is also found in comets and planets, as well as in galaxies where metals are extremely poor [17]. Therefore, polymeric CO may exist in planets, and is an important part in astrophysics research as well.

Pressure induction is an effective way to polymerize CO molecular crystals. Polymeric carbon monoxide (p-CO) has physical and chemical properties different from molecular crystals since the triple bond can be broken under pressure. Its polymerization temperature and pressure (4–5 GPa under laser irradiation, >80 K) [18,19] are much lower than that of pure nitrogen, thus, CO's polymerization is easily realized experimentally. Many scholars have studied the structures and characteristics of carbon monoxide at different pressures. In theory, Sun *et al.* [3,20] searched for some new polymerized carbon monoxide, such as the chainlike structure $Pna2_1$ under low pressure and the layered structure *Cmcm* under high pressure. Experimentally, Ryu *et al.* [21] showed a series of pressure-induced phase transitions of carbon monoxide. They speculated that the phase transition pressures from 1D $P2_1/m$ to 3D $I2_12_12_1$ and then to 2D *Cmcm* were about ∼7 GPa and ∼50 GPa, respectively. Apart from that, Ryu *et al.* [22] also found that hydrogen doping (∼10%) will accelerate the polymerization of carbon monoxide, which can greatly reduce the phase transformation pressures. Based on that research, they further explored chemical reactions of dense CO and H_2 (a wide range of H_2 concentration) at 9–30 GPa, and found a high-density COH_x network glass (∼3.23 g/cm^3) [23]. In addition, Dang *et al.* found that the morphology and stability of the pressure-induced extended solid of carbon monoxide depend on the rate of transformation, which is affected by pressure, volume per reaction area, and chemical catalysts [24]. Also, some researchers proposed that CO may form disproportionate carbon suboxide C_3O_2 at about 5 GPa, which will polymerize with further compression [9,25,26]. Lipp *et al.* [1] also found the vibrational band of CO_2 molecules by analyzing the Raman spectrum of the p-CO product at 5 GPa, and pointed out that the p-CO and the polymeric C_3O_2 ($(C_3O_2)_p$) have similar structures. Therefore, we infer that polymeric C_xO_y ($x > y$) may exist when considering the

*weiguo7@bit.edu.cn
†zhujl@sustech.edu.cn

mechanism of CO_2 release in *p*-CO. Meanwhile, considering the amorphous structure, metastability, and environmental sensitivity of the synthesized *p*-CO [1,21,27], it is rather difficult in experiment to characterize the fine structure of *p*-CO phase and predict new polymeric C_xO_y ($x > y$) phases.

In this work, through combinations of structural search, density functional theory (DFT) calculations and *ab initio* molecular dynamics simulations (AIMD), we find several polymeric C_xO_y ($x \geqslant y$) crystals in high pressures. For C : O ratio $= 1$ above 90 GPa, a layered structure, C_8O_8-I-4m2, is predicted to have lower enthalpy than known chainlike structure *Cmca* and layered structure *Cmcm*. The calculated energy density is 4.508 kJ/g. For C:O ratio > 1, we find three layered stable structures C_5O_2 (P-4m2) and C_6O_4(P-4m2 and I-4m2) above $40 \sim 50$ GPa. Remarkably, they all have energy density higher than 3 kJ/g, and are semiconductors with large bulk modulus and high hardness. We use AIMD to investigate the dynamic stability and possible phase transitions of the four C_xO_y structures at 0 GPa and 100 GPa, and find that C_8O_8-I-4m2 and C_6O_4-P-4m2 can transform into C_6O_4-I-4m2 and C_5O_2-P-4m2 by releasing CO_2 after pressure relief. Also, C_6O_4-I-4m2 and C_5O_2-P-4m2 are stable at ambient conditions. Phonon properties indicate that those structures are mechanically stable at 100 GPa, and their electronic band gaps are less affected by pressure due to larger bulk modulus.

II. COMPUTATIONAL METHODS

The DFT based structural search was performed to further predict new C_xO_y crystal structures, the method was implemented in the CALYPSO package, which is an efficient structure prediction method based on particle swarm optimization algorithm [28,29], and it only relies on the chemical ratio of given elements and external conditions to search ground and metastable states of studied systems. DFT calculations, using the projector augmented wave method [30,31], are performed in the Vienna *ab initio* simulation package (VASP) [32]. The electron exchange-correlation effects were described by the generalized gradient approximation (GGA) with the function of Perdew-Burke-Ernzerhof [33]. Also, van der Waals interaction in layered structures was included by DFT-D3 [34]. We have conducted variable-composition search at 0, 4, 10, 15, 60, 80, 100, 160, and 180 GPa, respectively. The number of C (O) atoms varies from 1 to 9. In the calculation, we use the same level of high precision setting as reported in Ref. [3] for the selection of the plane wave basis cutoff and pseudopotential (1050 eV, hard-version pseudopotential) to ensure the reliability of the results. Meanwhile, the convergence criteria of energy and force for structural optimization were set to 1×10^{-5} and 0.02 eV Å^{-1}, respectively.

In the simulations of *ab initio* molecular dynamics (MD), the NpT ensemble (constant pressure and temperature) was used to observe the dynamics of the structures. $3 \times 3 \times 3$ (189 atoms), $2 \times 2 \times 3$ (120 atoms) and $2 \times 2 \times 2$ (128 atoms) supercells for C_5O_2, C_6O_4 and C_8O_8 were used, respectively. Supercells were established based on the unit cell structures optimized at 0 GPa and 100 GPa. Simulations at each temperature ran to 6 ps with a time step of 1 fs. The Supplemental Material [35] Fig. S1 shows the energy changes of the four predicted C_xO_y crystals over time at 100 GPa and 300 K, indicating that the molecular dynamics of 6 ps time sufficiently reach the equilibrium state of the system. For mechanical studies, phonon frequency calculation was carried out within the PHONOPY code with the supercell method [36]. Anharmonic effect is important in properties like thermal conductivity and thermal expansion of solids, which is beyond the scope of this work, so we did not consider it in our phonon spectrum calculations. Elastic constants C_{ij} were obtained by using the stress-strain approach [37], which is based on analyzing changes in stress values caused by changes in the strain, elastic constants of strained materials can be accurately extracted by a symmetry-general approach for the least-squares. Since calculations of elastic constant are sensitive to the plane wave energy cutoff and the *k*-point distribution, we conducted a comparison test with C_5O_2-P-4m2 as a reference. The calculated results of the elastic constants C_{ij} of C_5O_2-P-4m2 at ambient pressure are shown in the Supplemental Material [35] Table S1, where we can see that the energy cutoff of 1050 eV and the *k*-point distribution of $18 \times 18 \times 6$ are sufficient for C_5O_2-P-4m2. The calculated elastic constants can be used to further calculate the bulk modulus B, shear modulus G, Young's modulus E and Poisson's ratio ν by the Voigt-Reuss-Hill approximations [38].

The relative enthalpies of C_xO_y crystals with different stoichiometric ratios were calculated with respect to C_8O_8-I-4m2 and CO_2 crystals,

$$\Delta H = \frac{H(C_xO_y) + H((x-y)CO_2)}{2x-y} - \frac{H(C_8O_8 - I - 4m2)}{8} \tag{1}$$

where C_xO_y and C_8O_8-I-4m2 are structures predicted in this work, except for $C_{16}O_{16}$-$Pna2_1$, $C_{16}O_{16}$-Cc, $C_{16}O_{16}$-*Cmca* and C_4O_4-*Cmcm* from the work of Sun *et al.* [3,20]. For CO_2, we have used the α-CO_2 (0 GPa) [39,40], CO_2-II (20 GPa), CO_2-V (40-200 GPa) [41] and layer-*AB* (220-300 GPa) [42,43] structures. Energy density is an essential parameter in studies of energetic materials. Here, we calculated the energy density of C_xO_y crystals (in unit of kJ/g) with respect to graphite and α-CO_2,

$$\rho(E) = \frac{E(8C_xO_y) - E((2x-y)C_4) - E(yC_4O_8)}{8(12x+16y)}, \tag{2}$$

where E is the internal energy at 0 GPa and 0 K, C_xO_y is the predicted structures, C_4 and C_4O_8 are the molecular formulas of graphite and α-CO_2 [39,40], respectively. Formation enthalpies of C_xO_y were calculated as

$$\Delta H_f = [H(C_xO_y) - xH(C) - yH(O)]/(x+y), \tag{3}$$

in which the graphite, diamond, α-O_2, ε-O_2 and ζ-O_2 structures are taken as the reference state for C and O in the corresponding pressures [44].

III. RESULTS AND DISCUSSION

Polymerized carbon monoxide is one of the potential HEDMs. Many researchers have focused on structures and properties of C_xO_y crystals with C : O = 1 : 1 [3,20–22,24].

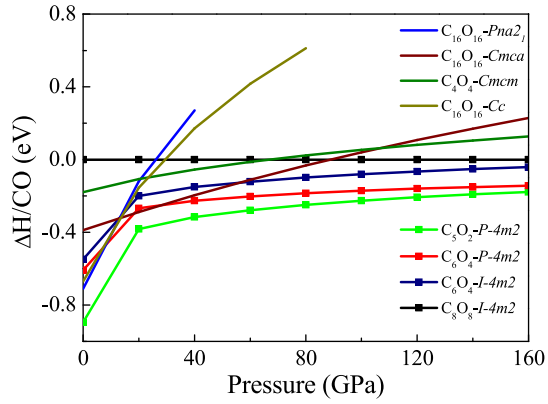

FIG. 1. Relative enthalpies of predicted C_xO_y crystals. Solid lines with symbols represent the three $C_xO_y + CO_2$ (C_xO_y: C_5O_2-*P*-4*m*2, C_6O_4-*P*-4*m*2, C_6O_4-*I*-4*m*2) systems and C_8O_8-*I*-4*m*2 phases that have the lowest relative enthalpies in our study. The enthalpy of C_8O_8-*I*-4*m*2 is set as the reference state. The structures of $C_{16}O_{16}$-*Pna*2$_1$, $C_{16}O_{16}$-*Cc*, $C_{16}O_{16}$-*Cmca* and C_4O_4-*Cmcm* are taken from the work of Sun *et al.* [3,20], and the enthalpies are recalculated and marked by solid lines in the figure.

Besides, we have also investigated the cases where $x > y$, all the lattice parameters of predicted C_xO_y crystals in this work are presented in the Supplemental Material [35] Table S2.

A. Crystal structures and energetics

The enthalpy-pressure relation can intuitively reflect the energy stability of structures and such a relation may give information about phase transition as pressure changes, which

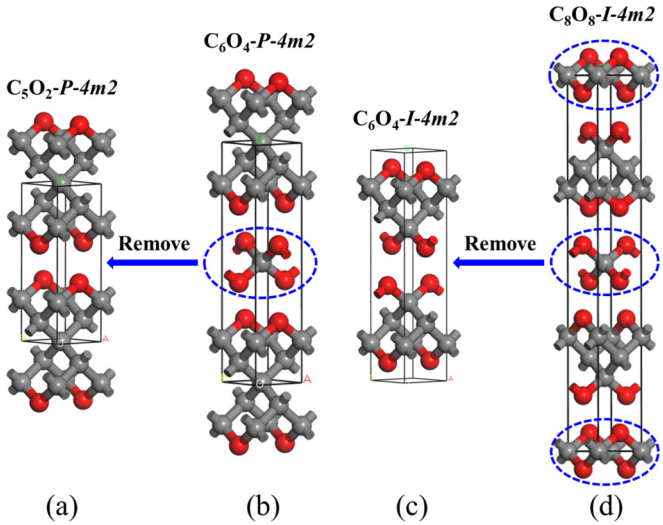

FIG. 2. The four C_xO_y crystals with the lowest relative enthalpies in high pressure of this work. (a) C_5O_2-*P*-4*m*2. (b) C_6O_4-*P*-4*m*2. (c) C_6O_4-*I*-4*m*2. (d) C_8O_8-*I*-4*m*2. The gray and red spheres denote carbon and oxygen atoms, respectively. The blue ovals and arrows indicate possible phase transition pathways from C_8O_8-*I*-4*m*2 to C_6O_4-*I*-4*m*2, and C_6O_4-*P*-4*m*2 to C_5O_2-*P*-4*m*2, by means of release of CO_2 molecules. The periodic structures surrounded by the ellipses are the monolayer structures of the high pressure phase layer-*AB* of CO_2 [42,43].

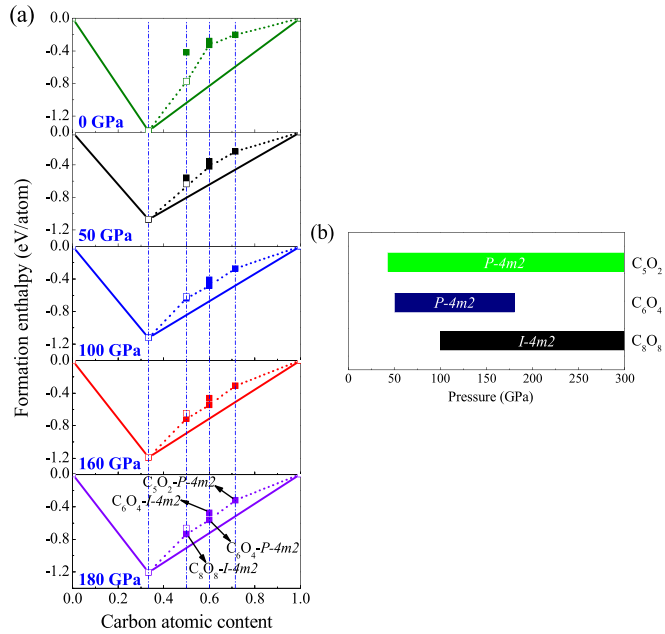

FIG. 3. (a) Formation enthalpies of C_xO_y phases with respect to elemental carbon and oxygen solids. The convex hulls connecting stable phases are shown by solid lines. Metastable phases are connected with dotted lines. The solid squares (■) are predicted structures in this work, which are enumerated as follows: C : O = 1 : 1 (C_8O_8-*I*-4*m*2), C : O = 6 : 4 (C_6O_4-*I*-4*m*2, C_6O_4-*P*-4*m*2 (lower formation enthalpy)), C : O = 5 : 2 (C_5O_2-*P*-4*m*2). The hollow squares (□) represent the recalculated results from published structures, α-CO_2 [39,40], CO_2-V [41], $C_{16}O_{16}$-*Pna*2$_1$, $C_{16}O_{16}$-*Cmca* and C_4O_4-*Cmcm* of CO [3,20], respectively. At different pressures, each structure remains the same symmetry, but the volume changes. (b) Predicted pressure-composition phase diagram of C_5O_2, C_6O_4 and C_8O_8.

is essential in the study of phase diagrams of condensed matter. Hence, we conduct a comparative analysis of the relative enthalpies of C_xO_y crystals, including the predicted structures (Supplemental Material [35] Table S2) and the reported structures [3,20]. We first focus on crystals of C : O = 1 : 1. As shown in Fig. 1, we can see that the most stable structure at ambient pressure is still the reported *Pna*2$_1$ [3]. At about 10 GPa, the polymeric structure of *Pna*2$_1$ undergoes a phase transformation and changes to the *Cc* phase. Next, the phase transition pressure from the *Cc* phase to the *Cmca* phase is about 13 GPa, and then the *Cmca* phase is transformed into *Cmcm* at pressure about 106 GPa, agreeing well with the values reported in the work of Sun *et al.* [3]. Moreover, we find a structure C_8O_8-*I*-4*m*2 with a lower enthalpy relative to the *Cmca* and the *Cmcm* phases at about 90 GPa. Thus, in terms of thermodynamics, we infer that when increasing the pressure of crystals of C : O ratio = 1 : 1, the phase transition path should be *Pna*2$_1$ → *Cc* → *Cmca* → *I*-4*m*2.

After considering the mechanism of CO_2 production during the process of forming *p*-CO [1], it is interesting to focus on possible new structures with C : O > 1. Figure 1 shows that compared to C_8O_8-*I*-4*m*2 in the corresponding pressure, the system of C_5O_2-*P*-4*m*2 and CO_2 crystals has the lowest relative enthalpy in this study from 20 up to 160 GPa, which

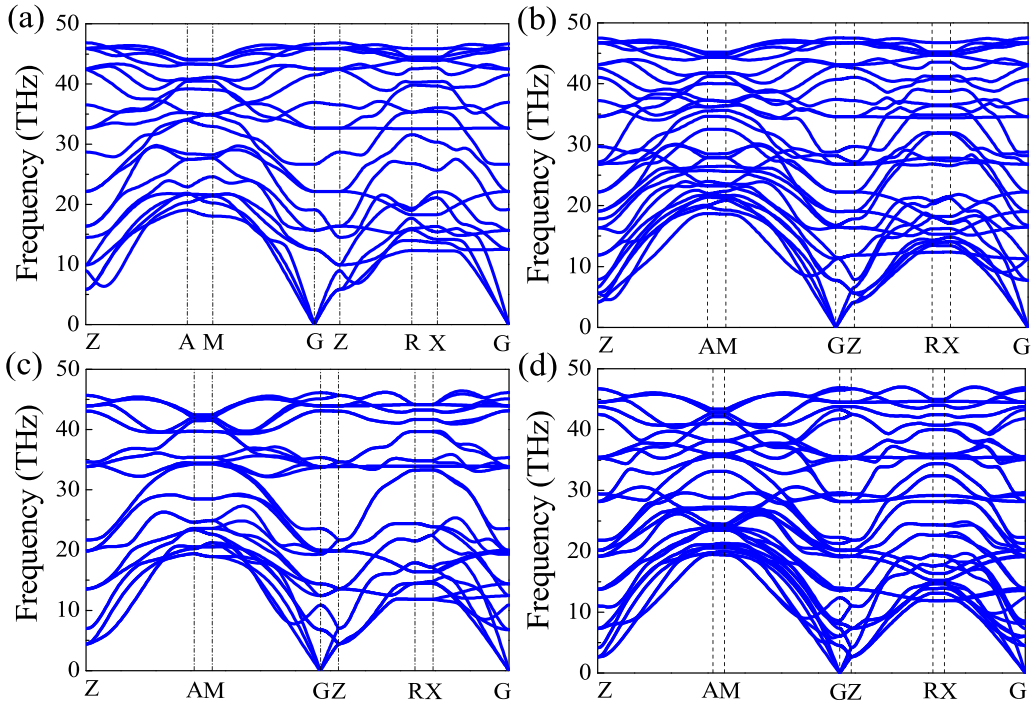

FIG. 4. Phonon dispersion curves at 100 GPa. (a) C_5O_2-P-4m2. (b) C_6O_4-P-4m2. (c) C_6O_4-I-4m2. (d) C_8O_8-I-4m2.

can be easily understood because CO is unstable relative to the $C_xO_y + CO_2$ system. The two phase, C_6O_4-P-4m2 and C_6O_4-I-4m2, are isomers, their ΔH are close to each other and lay in between that of C_5O_2-P-4m2 and C_8O_8-I-4m2. In addition, we can see that the relative enthalpies of C_5O_2-P-4m2 and C_6O_4-P-4m2, as well as C_6O_4-I-4m2 and C_8O_8-I-4m2 gradually tend to be the same as the pressure increases. That is because the enthalpy of the high pressure phase layer-AB [42,43] of CO_2 compensates for the enthalpy differences between them.

In addition to the structures in Fig. 1, we also find some other C_xO_y crystals, and their relative enthalpy calculations are included in the Supplemental Material [35] Fig. S3. The inset in Fig. S3 clearly shows that the enthalpies of C_9O-$P1 + CO$ (orange curve), C_5O_2-P-4m2 $+ CO_2$ (bright green curve) and C_8O_4-$C2/m + CO_2$ (purple curve) systems are lower than the $Pna2_1$ at 0 GPa. However, C_9O-$P1$ and C_8O_4-$C2/m$ are mechanically unstable at ambient pressure, and they can maintain mechanical stability only under high pressure (Supplemental Material [35] Fig. S4). Those structures (represented by dash-dotted lines) in Fig. S3 are also predicted ones. However, due to their higher enthalpies or mechanical instability at ambient pressure, we will not discuss them in detail here. The crystal structurers and lattice parameters are shown in Supplemental Material [35].

Figure 2 shows the crystal structures of C_5O_2-P-4m2, C_6O_4-P-4m2, C_6O_4-I-4m2, and C_8O_8-I-4m2, all of which are layered structures. The carbon and oxygen atoms are four-coordinated and two-coordinated, respectively. When decomposed into graphite and α-CO_2 [39,40] at ambient conditions, the calculated energy densities are as high as 3.474, 3.975, 4.314, and 4.508 kJ/g, respectively. C_5O_2-P-4m2 and C_6O_4-I-4m2 can be formed by removing CO_2 and $2CO_2$ (marked by blue dashed ovals in Fig. 2) from C_6O_4-P-4m2 and C_8O_8-I-4m2, respectively. As can be seen in Fig. 1, the ΔH of C_5O_2-P-4m2 and C_6O_4-P-4m2 tend to equalize as the pressure increase, and so do C_6O_4-I-4m2 and C_8O_8-I-4m2. The dynamics of the proposed transition process will be discussed in detail in the section of MD simulations.

Meanwhile, Fig. 3 shows the formation enthalpy of different compositions to indicate the phase stability of the p-C_xO_y compounds at 0, 50, 100, 160, and 180 GPa, respectively. The convex hulls connect the most stable structures via solid lines, while the dashed lines connect metastable structures above the solid lines. As can be seen from Fig. 3(a), when the carbon atomic content is 0.5, the formation enthalpy of the high-pressure phase (C_8O_8-I-4m2) predicted in this work is 0.073 eV/atom lower than the layered $Cmcm$ structure (reported in Ref. [20]) at 180 GPa. However, compared with $Pna2_1$ and $Cmca$, the formation enthalpy of C_8O_8-I-4m2 is higher at 0 and 50 GPa. The conclusions are consistent with the result shown in Fig. 1, that is, the phase transition path is $Pna2_1 \rightarrow Cc \rightarrow Cmca \rightarrow I-4m$2.

The predicted pressure-composition phase diagram shown in Fig. 3(b) indicates that, in the corresponding pressure range, the phases of C_5O_2-P-4m2, C_6O_4-P-4m2 and C_8O_8-I-4m2 have the lowest enthalpy under the same stoichiometric ratio. For instance, from 40 up to 300 GPa, C_5O_2-P-4m2 phase has the lowest enthalpy for C : O ratio $= 5 : 2$; for C : O ratio $= 6 : 4$, C_6O_4 is predicted to have P-4m2 symmetry between 50 and180 GPa; and the enthalpy of C_8O_8-I-4m2 is lowest at 100–300 GPa for C : O ratio $= 1 : 1$. Beyond 300 GPa, C_5O_2-P-4m2 and C_8O_8-I-4m2 are probably still the most stable phases. Although the predicted structures are above the solid line and maybe metastable, they are high-energy-density materials of polymeric C_xO_y crystals. Those structures enrich the phase diagram of high-pressure C_xO_y and we encourage

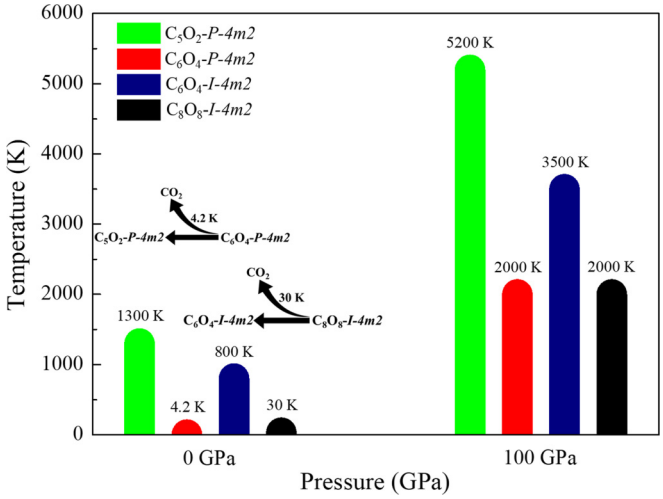

FIG. 5. The temperatures of the four predicted C_xO_y crystals at which the structures get unstable in AIMD simulations within 6 ps at 0 GPa and 100 GPa, respectively. The inset shows possible phase transitions route found from AIMD simulations within 6 ps at 0 GPa.

experimental and theoretical explorations of more powerful and stable polymeric C_xO_y crystals.

B. Mechanical stability, dynamic stability, and elastic properties

Studies of the phonon spectrum can characterize the mechanical stability of materials. As shown in Fig. 4, the phonon dispersion curves of the four C_xO_y structures have no any imaginary frequencies at 100 GPa, indicating that they are mechanically stable under high pressure. When recovered to ambient pressure, the phonon dispersion curves of the four C_xO_y crystals near the G point show some imaginary frequencies (Supplemental Material [35] Fig. S5), which may be caused by the lattice distortion in the Z direction after the pressure is released. As can be seen from Table S3, compared with 100 GPa, the lattice parameter $a = b$ at 0 GPa has a small change, while c has a significant change. Also, there is very little dispersion along the *A-M, G-Z* and *R-X* directions at ambient pressure, so the interlayer interaction is weak after pressure releasing.

Then, we use MD simulations to study the evolution of C_5O_2-*P*-4*m*2, C_6O_4-*P*-4*m*2, C_6O_4-*I*-4*m*2 and C_8O_8-*I*-4*m*2 under NpT ensemble, the structures under 0 and 100 GPa at various temperatures are shown in the Supplemental Material [35] Fig. S6 and Fig. S7, and in Fig. 5 we summarize the temperatures at which the structures become unstable within 6 ps. Due to the limitations in simulation time and supercell size, we can only take the height of the temperature bar as an indication of its dynamic stability, rather than its phase transition temperature. We can see that the rank of the dynamic stability of the four predicted C_xO_y crystals is C_5O_2-*P*-4*m*2 > C_6O_4-*I*-4*m*2 > C_8O_8-*I*-4*m*2 ⩾ C_6O_4-*P*-4*m*2 for both 0 and 100 GPa. Among them, C_5O_2-*P*-4*m*2 is always the most stable one; the relatively poor dynamic stabilities of C_6O_4-*P*-4*m*2 and C_8O_8-*I*-4*m*2 are due to the presence of the high-pressure phase of CO_2 (single-layered form) in their crystal structures, so they are easier to decompose than C_6O_4-*I*-4*m*2 and C_5O_2-*P*-4*m*2, which is more obvious under 0 GPa.

The inset in Fig. 5 shows the possible phase transition route between the four predicted C_xO_y crystals at 0 GPa, where the single-layered structures, i.e., the high-pressure layer-*AB* phase of CO_2 in C_6O_4-*P*-4*m*2 and C_8O_8-*I*-4*m*2, start to decompose into CO_2 at ∼4.2 K (the liquefaction temperature of helium [45]) and ∼30 K, respectively, and then they transform into C_5O_2-*P*-4*m*2 and C_6O_4-*I*-4*m*2. Although C_6O_4-*P*-4*m*2 has lower enthalpy compared to C_6O_4-*I*-4*m*2, there is no structural transform between them observed in MD, so we infer that transition between the two phases of C_6O_4 requires maintaining a certain high pressure and high temperature, so that the crystal can be sufficiently relaxed to a structure with lower enthalpy. MD simulations show that the high-pressure phase of CO_2 tends to convert into CO_2 molecules after pressure release, which is consistent with the fact that CO_2 exists in the form of molecular crystals at atmospheric pressure [39,40]. Under 0 GPa, C_5O_2-*P*-4*m*2 and C_6O_4-*I*-4*m*2 become disordered at about 1300 and 800 K, respectively. The structural details can be seen in the Supplemental Material [35] Fig. S6. At 100 GPa, the four C_xO_y crystals' dynamic stability is greatly enhanced, C_6O_4-*P*-4*m*2 and C_8O_8-*I*-4*m*2 phases

TABLE I. Calculation results of bulk modulus B (GPa), shear modulus G (GPa), G/B, Young's modulus E (GPa), Poisson's ratio ν, and Vickers hardness H_v (GPa) for C_5O_2-*P*-4*m*2, C_6O_4-*P*-4*m*2, C_6O_4-*I*-4*m*2 and C_8O_8-*I*-4*m*2 compared with *c*-BN and diamond at 0 GPa. $B_V(G_V)$ and $B_R(G_R)$ are the values of the bulk modulus (shear modulus) using Voigt theory and Reuss theory, which are the upper and lower limits of bulk modulus (shear modulus), respectively; and $B(G)$ is the average of $B_V(G_V)$ and $B_R(G_R)$.

	C_5O_2-*P*-4*m*2	C_6O_4-*P*-4*m*2	C_6O_4-*I*-4*m*2	C_8O_8-*I*-4*m*2	*c*-BN [56]	Diamond [56]
B_0 (EoS)	198.150	183.484	179.282	174.265		
B_V	195.963	182.208	179.830	176.871		
B_R	41.604	33.969	36.871	38.030		
B	118.784	108.089	108.350	107.450	376	445
G_V	168.573	151.512	145.825	137.358		
G_R	14.751	16.275	13.488	15.521		
G	91.662	83.893	79.657	76.439	322	490
G/B	0.772	0.776	0.735	0.711	0.86	1.10
E	218.725	199.950	191.934	185.363	751	1075
ν	0.193	0.192	0.205	0.212	0.166	0.097
H_v	30.604	23.938	23.250	19.217	67.7	98

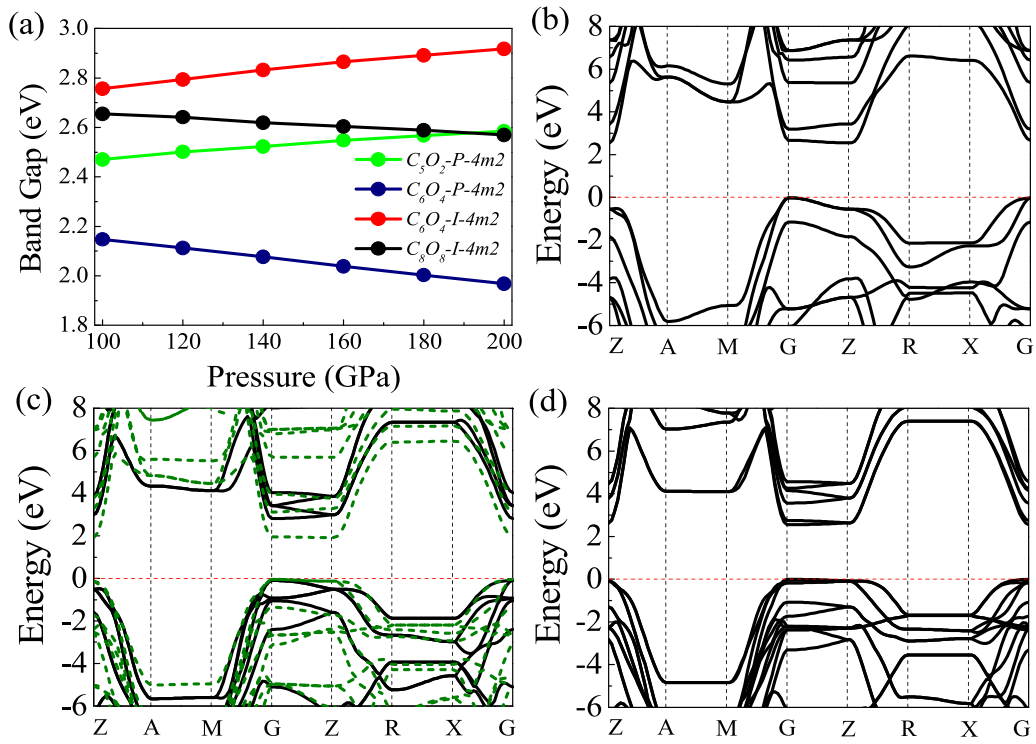

FIG. 6. Electronic band structures of the four predicted C_xO_y crystals. (a) Pressure dependence of electronic band gaps. (b) Band structure of C_5O_2-*P*-4*m*2 at 200 GPa. (c) Band structures of C_6O_4-*I*-4*m*2 (black) and C_6O_4-*P*-4*m*2 (olive) at 200 GPa. (d) Band structure of C_8O_8-*I*-4*m*2 at 200 GPa.

start to disorder at around 2000 K, other structures are even more stable. The structural evolutions in MD after 6 ps at 100 GPa and various temperatures are shown in the Supplemental Material [35] Fig. S7, and the lattice parameters of the systems are shown in the Supplemental Material [35] Table S4. Thus, our AIMD simulations indicate that the four C_xO_y crystals are all stable at high pressures, and the structures of C_5O_2-*P*-4*m*2 and C_6O_4-*I*-4*m*2 can be probably maintained when recovered to ambient conditions.

Besides the calculation of phonon curves, the study of elastic stability is also essential for the characterization of mechanical properties. The crystals in the tetragonal system have six independent elastic constants, namely C_{11}, C_{12}, C_{13}, C_{33}, C_{44}, and C_{66}. For the mechanically stable structures in the tetragonal system, it should satisfy the generalized criteria: $C_{11} > 0$, $C_{33} > 0$, $C_{44} > 0$, $C_{66} > 0$, $(C_{11} - C_{12}) > 0$, $(C_{11} + C_{33}\text{-}2C_{13}) > 0$, and $[2(C_{11} + C_{12}) + C_{33} + 4C_{13}] > 0$ [46]. The elastic constants of C_5O_2-*P*-4*m*2, C_6O_4-*P*-4*m*2, C_6O_4-*I*-4*m*2 and C_8O_8-*I*-4*m*2 at 0 GPa are shown in the Supplemental Material [35] Table S1 and Table S5, respectively, which also confirms their mechanical stability. The bulk modulus B, shear modulus G, Young's modulus E and Poisson's ratio ν are shown in Table I. Meanwhile, we also used the Birch-Murnaghan equation of state (EoS) [47] to fit the bulk modulus B_0 (Supplemental Material [35] Fig. S8), which is close to the B_V and much larger than bulk moduli of TNT (∼5 GPa), β-HMX (∼7 GPa), ε-CL-20(∼10 GPa) [48–51] and transition metal carbohydrazide perchlorate complexes (∼18 GPa) [52], so the four C_xO_y crystals have greater rupture strength compared with traditional energetic materials. The discrepancy between B_0 and B_V may result from the different relaxation conditions used in the energy-strain and stress-strain methods [53–55]. For Table I, we can also see that the four energetic materials have a large bulk modulus, shear modulus and Young's modulus, and the G/B ratio is greater than 0.57, indicating that they are stiff materials with a brittle nature [6,57,58]. The Poisson's ratio is less than 0.33, reflecting the characteristic of covalent bonding [59].

Considering that C_5O_2-*P*-4*m*2, C_6O_4-*P*-4*m*2, C_6O_4-*I*-4*m*2 and C_8O_8-*I*-4*m*2 are hard materials, therefore the calculation of hardness is essential. Here, we used the Gao's model to calculate the Vickers hardness H_v [60,61].

$$H_v = \left[\prod^{\mu}\left(740P^{\mu}\nu_b^{\mu^{-5/3}}\right)^{n^{\mu}}\right]^{1/\sum n^{\mu}} = \left[\prod^{\mu}\left(H_v^{\mu}\right)^{n^{\mu}}\right]^{1/\sum n^{\mu}}, \tag{4}$$

where

$$\nu_b^{\mu} = (d^{\mu})^3 \Big/ \sum_{\nu}\left[(d^{\nu})^3 N_b^{\nu}\right], \tag{5}$$

P^{μ} is the Mulliken overlap population of the μ-type bond, n^{μ} is the number of μ-type bond in the unit cell, d^{μ} is the bond length of μ-type, and N_b^{ν} is the number of μ-type bond per unit volume. Compared with C_6O_4-*P*-4*m*2, C_6O_4-*I*-4*m*2 and C_8O_8-*I*-4*m*2, C_5O_2-*P*-4*m*2 has a larger Vickers hardness (30.604 GPa), and although the hardness is much lower than typical superhard materials (Diamond and *c*-BN), it is comparable to that of AlN_5 nitrides of high-energy-density

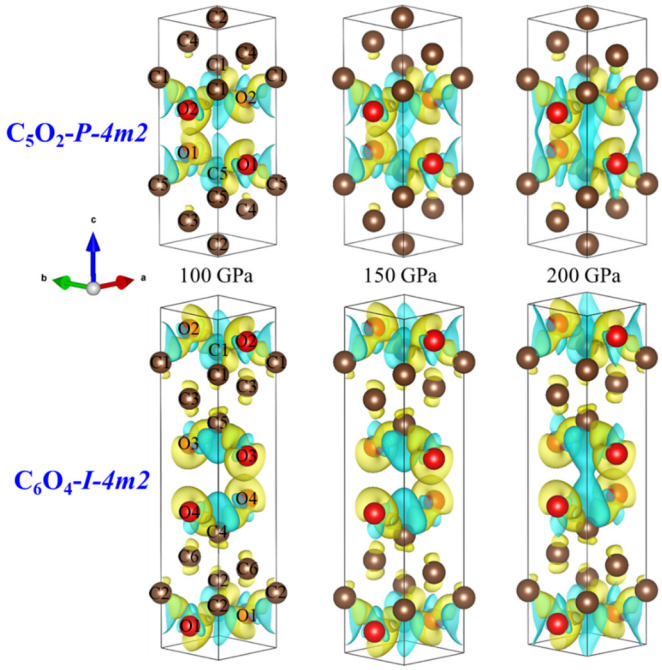

FIG. 7. Plot of charge density difference (e • Å^{-3}, crystal's electron density minus the superposition of the electron densities of separate C and O atoms) of C_5O_2-*P*-4*m*2 and C_6O_4-*I*-4*m*2 at 100 GPa, 150 GPa and 200 GPa, respectively. Isosurface level = 0.12. Blue region means electron deficiency, and yellow region indicates electron accumulation.

materials [62]. As a kind of high-energy-density material with high hardness, C_5O_2-*P*-4*m*2, C_6O_4-*P*-4*m*2, C_6O_4-*I*-4*m*2 and C_8O_8-*I*-4*m*2 have a strong ability to resist deformation destruction.

C. Electronic structures

Electronic properties play an important role in the characterization of materials' properties. Here, we first focus on the band structures of the four predicted C_xO_y phases. Electronic band gap is sensitive to applied external pressures, so the dependence of band gap on pressure is studied. As shown in Fig. 6(a), the band gaps of C_6O_4-*P*-4*m*2 and C_8O_8-*I*-4*m*2 gradually decrease with increasing pressure, but they still maintain nonmetallic in nature with band gaps of 1.968 eV [Fig. 6(c)] and 2.569 eV [Fig. 6(d)] at 200 GPa, respectively. It is well known that GGA or local density approximation functionals tend to underestimate the band gap of many semiconductors, so we infer that their metallization pressure should be higher than 200 GPa. In the meantime, we can see that the band gaps of C_6O_4-*P*-4*m*2 and C_8O_8-*I*-4*m*2 are less dependent on pressure compared with systems showing pressure-induced insulator-metal transitions [63–67]. Combining the comparison of the lattice parameters and volumes under different pressures in the Supplemental Material [35] Table S6, as well as the calculated elastic properties of the four predicted C_xO_y crystals, we infer that the reason is, the bulk moduli of the crystals are large, so that the lattice does not change dramatically, which in turn leads to a small change in the band gaps with pressure. Such weak dependence is similar to the polymerized nitrogen $P2_12_12_1$ in the work of Ma *et al.* [68], where the band gap of $P2_12_12_1$ phase decreases from 2.64 to 2.57 eV with an increase of pressure from 350 to 500 GPa.

Surprisingly, the band gaps of C_5O_2-*P*-4*m*2 and C_6O_4-*I*-4*m*2 gradually increase with further compression [Fig. 6(a)]. From the partial band structures (Supplemental Material [35] Fig. S9 and S10), we can see that the valence bands of C_5O_2-*P*-4*m*2 and C_6O_4-*I*-4*m*2 are mainly from the p_x and p_y orbitals of O atoms, the conduction band of C_5O_2-*P*-4*m*2 mainly arises from the p_z orbitals of C1 and C5 atoms, and the p_z orbitals of C1, C2, C4, and C5 contribute to the conduction band of C_6O_4-*I*-4*m*2. The results are verified in the calculation of the charge density difference. As shown in Fig. 7, the cruising electrons in the gaps of C layers are gradually transferred to the interlayer of C-O atoms with further compression, resulting in enhanced localization of electrons, which in turn will increase the band gap. A similar mechanism has also been mentioned in the study of pressure-induced metal-insulator transition in Na reported by Ma *et al.* [69], where a strong localization of valence electrons in the interstices of the hP4 phase of Na is responsible for the transition, and Na-hP4 exhibits insulating properties under 300 GPa.

IV. CONCLUSION

Through combinations of DFT based structural search and AIMD simulations, we have found a few C_xO_y polymers and focused on four layered structures C_5O_2-*P*-4*m*2, C_6O_4 (*P*-4*m*2 and *I*-4*m*2) and C_8O_8-*I*-4*m*2, whose energy densities are 3.474, 3.975, 4.314, and 4.508 kJ/g, respectively. When C:O ratio is equal to 1, the predicted structure, i.e., C_8O_8-*I*-4*m*2, has an energy density higher than TNT (4.3 kJ/g). We find that above 90 GPa, the enthalpy of C_8O_8-*I*-4*m*2 is lower than the known chainlike structure *Cmca* and the layered structure *Cmcm*. Thus, we infer that when increasing the pressure, the phase transition path should be $Pna2_1 \rightarrow Cc \rightarrow Cmca \rightarrow I\text{-}4m2$ for C : O ratio $= 1$. Moreover, when considering the CO_2 release in the crystals, we have also predicted structures with C : O > 1, in which C_5O_2-*P*-4*m*2 is the structure with the lowest enthalpy above 40 GPa for C : O ratio $= 5 : 2$, and it is also a hard material with a high Vickers hardness of 30.6 GPa and bulk modulus of nearly 200 GPa. The phonon spectrum calculation shows its good mechanical stability. AIMD simulations give the rank of dynamic stability of the four predicted C_xO_y crystals at 0 GPa and 100 GPa, namely C_5O_2-*P*-4*m*2 $>$ C_6O_4-*I*-4*m*2 $>$ C_8O_8-*I*-4*m*2 $\geqslant$ C_6O_4-*P*-4*m*2. AIMD simulations also provide information about the possible phase transformation route: C_8O_8-*I*-4*m*2 and C_6O_4-*P*-4*m*2 to C_6O_4-*I*-4*m*2 and C_5O_2-*P*-4*m*2 through the release of CO_2 at 0 GPa, respectively. C_5O_2-*P*-4*m*2 and C_6O_4-*I*-4*m*2 can remain stable at ambient conditions. In addition, we have conducted research on the electronic properties, and they are all semiconductors. Large bulk moduli cause their electronic band gaps to be less sensitive to pressure. The partial band structures and the plot of charge density difference explain well that the abnormal band gap behavior of C_5O_2-*P*-4*m*2 and C_6O_4-*I*-4*m*2 (the band gaps increase with increasing pressure) is due to the enhanced

localization of electrons in the interlayer of C-O atoms with further compression. To conclude, we have predicted four layered p-C_xO_y structures, and studied their crystal structures, energetics, mechanical and dynamic stability, elastic properties, and electronic structures. This work provides clues for synthesis and exploration of new energetic materials besides polymeric nitrogen.

ACKNOWLEDGMENTS

This work was supported by the National Natural Science Foundation of China (NSFC, Grant No. 51971037) and National Key Research and Development Program of China (No. 2017YFB0701603), and the open funding of Xi'an Modern Chemistry Research Institute (Grants No. SYJJ200303).

[1] M. J. Lipp, W. J. Evans, B. J. Baer, and C. S. Yoo, Nat. Mater. **4**, 211 (2005).
[2] Z. Raza, C. J. Pickard, C. Pinilla, and A. M. Saitta, Phys. Rev. Lett. **111**, 235501 (2013).
[3] K. Xia, J. Sun, C. J. Pickard, D. D. Klug, and R. J. Needs, Phys. Rev. B **95**, 144102 (2017).
[4] T. M. Klapötke, Struct. Bond. **125**, 85 (2007).
[5] Q. Li, H. Liu, D. Zhou, W. Zheng, Z. Wu, and Y. Ma, Phys. Chem. Chem. Phys. **14**, 13081 (2012).
[6] R. B. Kaner, J. J. Gilman, and S. H. Tolbert, Science **308**, 1268 (2005).
[7] N. W. Ashcroft, Phys. Rev. Lett. **92**, 187002 (2004).
[8] M. Lipp, W. J. Evans, V. Garcia-Baonza, and H. E. Lorenzana, J. Low Temp. Phys. **111**, 247 (1998).
[9] S. Bernard, G. L. Chiarotti, S. Scandolo, and E. Tosatti, Phys. Rev. Lett. **81**, 2092 (1998).
[10] C. Mailhiot, L. H. Yang, and A. K. McMahan, Phys. Rev. B **46**, 14419 (1992).
[11] J. Sun, M. Martinez-Canales, D. D. Klug, C. J. Pickard, and R. J. Needs, Phys. Rev. Lett. **111**, 175502 (2013).
[12] D. Scelta, K. F. Dziubek, M. Ende, R. Miletich, M. Mezouar, G. Garbarino, and R. Bini, Phys. Rev. Lett. **126**, 065701 (2021).
[13] C. S. Yoo, H. Cynn, F. Gygi, G. Galli, V. Iota, M. Nicol, S. Carlson, D. Häusermann, and C. Mailhiot, Phys. Rev. Lett. **83**, 5527 (1999).
[14] J. Sun, M. Martinez-Canales, D. D. Klug, C. J. Pickard, and R. J. Needs, Phys. Rev. Lett. **108**, 045503 (2012).
[15] R. L. Mills, B. Olinger, and D. T. Cromer, J. Chem. Phys. **84**, 2837 (1986).
[16] L. Wang, C. Sun, H. Xu, J. Zhang, Y. Zhao, W. Guo, and J. Zhu, AIP Adv. **10**, 045301 (2020).
[17] Y. Shi, J. Wang, Z.-Y. Zhang, Y. Gao, C.-N. Hao, X.-Y. Xia, and Q. Gu, Nat. Commun. **7**, 13789 (2016).
[18] D. T. Cromer, D. Schiferl, R. Lesar, and R. L. Mills, Acta Crystallogr. Sect. C **C39**, 1146 (1983).
[19] A. I. Katz, D. Schiferl, and R. L. Mills, J. Phys. Chem. **88**, 3176 (1984).
[20] J. Sun, D. D. Klug, C. J. Pickard, and R. J. Needs, Phys. Rev. Lett. **106**, 145502 (2011).
[21] Y.-J. Ryu, M. Kim, J. Lim, R. Dias, D. Klug, and C.-S. Yoo, J. Phys. Chem. C **120**, 27548 (2016).
[22] Y.-J. Ryu, C.-S. Yoo, M. Kim, X. Yong, J. S. Tse, S. K. Lee, and E. J. Kim, J. Phys. Chem. C **121**, 10078 (2017).
[23] Y. J. Ryu, C.-S. Yoo, J. Lim, M. Kim, X. Yong, and J. S. Tse, J. Phys. Chem. C **124**, 107 (2020).
[24] N. C. Dang and J. A. Ciezak-Jenkins, J. Chem. Phys. **148**, 144702 (2018).
[25] R. L. Mills, D. Schiferl, A. I. Katz, and B. W. Olinger, J. Phys. Colloq. **45**, C8 (1984).
[26] N.-L. Yang, A. Snow, and H. Haubenstock, J. Polym. Sci. Polym. Chem. Ed. **16**, 1909 (1978).
[27] W. J. Evans, M. J. Lipp, C.-S. Yoo, H. Cynn, J. L. Herberg, and R. S. Maxwell, Chem. Mater. **18**, 2520 (2006).
[28] Y. Wang, J. Lv, L. Zhu, and Y. Ma, Comput. Phys. Commun. **183**, 2063 (2012).
[29] Y. Wang, J. Lv, L. Zhu, and Y. Ma, Phys. Rev. B **82**, 094116 (2010).
[30] P. E. Blöchl, Phys. Rev. B **50**, 17953 (1994).
[31] G. Kresse and D. Joubert, Phys. Rev. B **59**, 1758 (1999).
[32] G. Kresse and J. Furthmüller, Phys. Rev. B **54**, 11169 (1996).
[33] J. P. Perdew, K. Burke, and M. Ernzerhof, Phys. Rev. Lett. **77**, 3865 (1996).
[34] S. Grimme, S. Ehrlich, and L. Goerigk, J. Comput. Chem. **32**, 1456 (2011).
[35] See Supplemental Material at http://link.aps.org/supplemental/10.1103/PhysRevB.104.094102 for lattice parameters and atomic position information of the predicted structures at selected pressures, phonon dispersion curves, elastic constant Cij, the bulk modulus by fitting the Birch-Murnaghan EoS, partial band structures and details of AIMD after 6 ps of the four predicted CxOy crystals.
[36] A. Togo and I. Tanaka, Scr. Mater. **108**, 1 (2015).
[37] Y. Le Page and P. Saxe, Phys. Rev. B **65**, 104104 (2002).
[38] R. Hill, Proc. Phys. Soc. A **65**, 349 (1952).
[39] Y. Han, J. Liu, L. Huang, X. He, and J. Li, Npj Quant. Mater. **4**, 10 (2019).
[40] C.-S. Yoo, Phys. Chem. Chem. Phys. **15**, 7949 (2013).
[41] B. H. Cogollo-Olivo, S. Biswas, S. Scandolo, and J. A. Montoya, Phys. Rev. Lett. **124**, 095701 (2020).
[42] M.-S. Lee, J. A. Montoya, and S. Scandolo, Phys. Rev. B **79**, 144102 (2009).
[43] S. Serra, C. Cavazzoni, G. L. Chiarotti, S. Scandolo, and E. Tosatti, Science **284**, 788 (1999).
[44] Y. Ma, A. R. Oganov, and C. W. Glass, Phys. Rev. B **76**, 064101 (2007).
[45] H. K. Onnes, Proc. R. Netherlands Acad. Arts Sci. (KNAW) **11**, 168 (1908).
[46] Z.-J. Wu, E.-J. Zhao, H.-P. Xiang, X.-F. Hao, X.-J. Liu, and J. Meng, Phys. Rev. B **76**, 054115 (2007).
[47] F. Birch, Phys. Rev. **71**, 809 (1947).
[48] G.-Y. Hang, W.-L. Yu, T. Wang, and J.-T. Wang, J. Mol. Model. **25**, 10 (2019).
[49] G.-Y. Hang, W.-L. Yu, T. Wang, J.-T. Wang, and Z. Li, J. Mol. Model. **23**, 362 (2017).
[50] T. Sun, J. J. Xiao, Q. Liu, F. Zhao, and H. M. Xiao, J. Mater. Chem. A **2**, 13898 (2014).
[51] G.-y. Hang, W.-l. Yu, T. Wang, J.-t. Wang, and Z. Li, J. Mol. Model. **23**, 281 (2017).

[52] C. Sun, W. Zhang, Y. Lü, F. Wang, W. Guo, T. Zhang, and Y. Yao, Phys. Chem. Chem. Phys. **21**, 24034 (2019).
[53] S. Shang, Y. Wang, and Z.-K. Liu, Appl. Phys. Lett. **90**, 101909 (2007).
[54] S. L. Shang, Y. Wang, D. E. Kim, C. L. Zacherl, Y. Du, and Z. K. Liu, Phys. Rev. B **83**, 144204 (2011).
[55] S.-L. Shang, L. G. H. Jr, S. Shi, Y. Qi, Y. Wang, and Z.-K. Liu, Acta Mater. **60**, 5204 (2012).
[56] F. Tian, J. Wang, Z. He, Y. Ma, L. Wang, T. Cui, C. Chen, B. Liu, and G. Zou, Phys. Rev. B **78**, 235431 (2008).
[57] S. F. Pugh, Philos. Mag. **45**, 823 (1954).
[58] S. Ma, F. Peng, S. Zhu, S. Li, and T. Gao, J. Phys. Chem. C **122**, 22660 (2018).
[59] G. N. Greaves, A. L. Greer, R. S. Lakes, and T. Rouxel, Nat. Mater. **10**, 823 (2011).
[60] F. Gao, J. He, E. Wu, S. Liu, D. Yu, D. Li, S. Zhang, and Y. Tian, Phys. Rev. Lett. **91**, 015502 (2003).
[61] F. Gao, Phys. Rev. B **73**, 132104 (2006).
[62] Z. Liu, D. Li, Y. Liu, T. Cui, F. Tian, and D. Duan, Phys. Chem. Chem. Phys. **21**, 12029 (2019).
[63] M. Kim, M. Debessai, and C.-S. Yoo, Nat. Chem. **2**, 784 (2010).
[64] R. P. Dias, C.-S. Yoo, V. V. Struzhkin, M. Kim, T. Muramatsu, T. Matsuoka, Y. Ohishi, and S. Sinogeikin, Proc. Natl. Acad. Sci. U. S. A. **110**, 11720 (2013).
[65] R. P. Dias and I. F. Silvera, Science **355**, 715 (2017).
[66] R. P. Dias, C.-S. Yoo, M. Kim, and J. S. Tse, Phys. Rev. B **84**, 144104 (2011).
[67] R. Reichlin, K. E. Brister, A. K. McMahan, M. Ross, S. Martin, Y. K. Vohra, and A. L. Ruoff, Phys. Rev. Lett. **62**, 669 (1989).
[68] Y. Ma, A. R. Oganov, Z. Li, Y. Xie, and J. Kotakoski, Phys. Rev. Lett. **102**, 065501 (2009).
[69] Y. Ma, M. Eremets, A. R. Oganov, Y. Xie, I. Trojan, S. Medvedev, A. O. Lyakhov, M. Valle, and V. Prakapenka, Nature (London) **458**, 182 (2009).